This is a pre-print of the article:

Inthamoussou, F. A., J. Pegueroles-Queralt, and F. D. Bianchi. "Control of a supercapacitor energy storage system for microgrid applications". *IEEE Transactions on Energy Conversion*, vol. 28, no. 3, pp. 690–697, 2013.

DOI: 10.1109/TPWRD.2011.2144625

IEEEXplore Digital Library: http://ieeexplore.ieee.org/xpl/articleDetails.jsp?arnumber=6517491

Control of a supercapacitor energy storage system for microgrid applications

Fernando A. Inthamoussou, *Student Member, IEEE*, Jordi Pegueroles-Queralt and Fernando D. Bianchi

***Abstract*—The proper operation of a microgrid requires storage devices that increase the inertia and avoid instability of the system. This article presents the control of an energy storage system (ESS) based on supercapacitors in the context of grid-connected microgrids. The ESS is composed of AC/DC and DC/DC converters tied by a DC link. A single sliding mode strategy is proposed to control a bidirectional DC/DC converter, capable of working properly under all operating conditions. The switching devices are commanded by a single sliding function, dynamically shaped by references sent from the microgrid central controller. This feature facilitates the implementation and design of the control law and simplifies the stability analysis over the entire operating range. The effectiveness of the proposed control strategy is illustrated by experimental results.**

***Index Terms*—Supercapacitors, energy storage systems, microgrids, power electronics, sliding mode control, experimental setup, nonlinear control**

I. Introduction

MICROGRIDS are emerging solutions that provide eco-friendly energy systems. In the near future microgrids will penetrate into power systems, especially in electric power distribution grids [1], [2], delivering clean and renewable power close to the end customers [3]. A microgrid is composed of a number of controllable micro-sources and controllable loads. According to the operation requirements, the microgrid can be connected (grid-connected mode) [4] or disconnected (islanding mode) from the utility grid [5]. During the grid-connected operation, active and reactive power references are assigned by the microgrid central controller (MGCC) [6].

Power generators in microgrids are generally interfaced with power electronics, enabling a new flexible way to manage the power flow [7]. The electronic interfaces are split into two power converters in a back-to-back topology, tied by a DC-link, with the grid side converter (GSC) and the micro-source side converter. A power system dominated by power electronic interfaces has very low rotating mass inertia, which can lead to a unstable system. By adding energy storage systems (ESS), the equivalent inertia introduced increases the robustness of the system, making it more immune to perturbations, such as changes in the loading conditions or changes in the electric energy production due to atmospheric variability [8]. There are many possible technologies to implement an energy storage system: batteries, flywheels, superconducting magnetic energy storage SMES, supercapacitors and others [9]. None of these technologies offer a clear advantage over the others. To provide the power and storage capabilities required by the microgrid, a hybrid solution is commonly adopted [8]. For this work, the focus will be in supercapacitors, but the same concepts can be applied to batteries.

In the context of microgrids, an ESS based on supercapacitors consists of a GSC and a bidirectional DC/DC converter (energy storage side converter, ESSC). In the case of grid connected microgrids, the GSC is a voltage source converter that ensures the power transfer between the microgrid and the ESS by regulating the voltage of the DC link. The control of this converter has been extensively treated, see *e.g.* [10]–[12]. The control of bidirectional DC/DC converters has been widely analyzed in the literature, but not so extensively in microgrid applications. Among other control techniques, nonlinear techniques based on variable structures systems (VSS) and sliding mode (SM) theories result especially suitable for switched systems like power converters [13], [14]. Sliding mode techniques permit the combination of designs with different objectives and also provide a quite simple implementation. Therefore, for power converters subjected to high variable operating conditions, SM algorithms become a natural choice considering their large signal capability.

Several articles have analyzed and proposed SM control strategies for DC/DC converters in a variety of applications, for example [15]–[21]. Although, the use of bidirectional DC/DC converters controlled by SM to ensure a proper power exchange in a microgrids is not common. In [15], [17], [19], unidirectional converters with resistive loads as a single isolated stage are analyzed. For example, [17] presents the control of a high voltage two-cell buck converter, where SM is used to control the inductor current and a PI control is added to regulate the output voltage. This configuration is unidirectional in power and the results are evaluated by numerical simulations. In [18] a bidirectional buck-derived converter is controlled by hysteresis to extend the battery life through the charge/discharge of a supercapacitor. In [20], the SM control of a coupled inductor bidirectional DC/DC converter is addressed and results are presented by simulations for a DC tramway application. Stability analyses are not addressed in [15], [17]–[20]. In [16] and [21] stability analyses are performed on unidirectional converters as isolated stages.

The main contribution of this article is to propose an SM

F. A. Inthamoussou is with CONICET, LEICI-FI-UNLP, Calle 48 y 116, CC 91 (1900), La Plata, Buenos Aires, Argentina

J. Pegueroles-Queralt and F. D. Bianchi are with the Catalonia Institute for Energy Research, IREC, Jardins de les Dones de Negre 1, 08930 Sant Adrià de Besòs (Barcelona), Spain

The research of F.A. Inthamoussou was supported by CONICET (PIP 00361 2012/14) and UNLP (11/I164 2012/15).

The research of J. Pegueroles-Queralt and F.D. Bianchi was supported by the EIT and KIC-InnoEnergy under the Project KIC-SMART POWER (31_2011_IP27_Smart Power) and by the European Regional Development Funds (ERDF, "FEDER Programa Competitivitat de Catalunya 2007-2013").

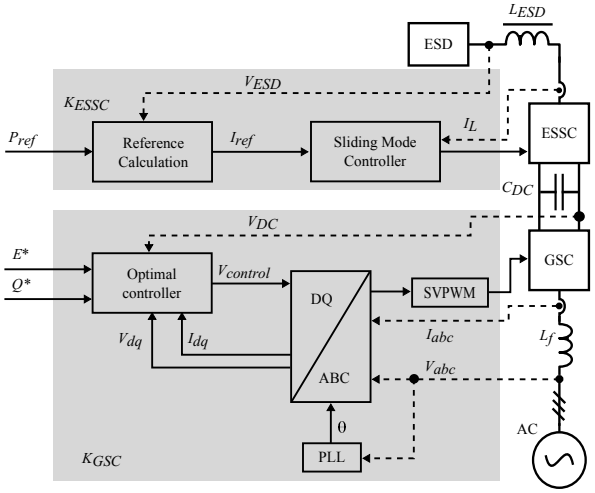

Fig. 1. Adopted interface topology for ESS and the power grid

control strategy for a bidirectional DC/DC converter for an ESS based on supercapacitors in the context of microgrid applications. The strategy covers all operating conditions: startup, constant power and voltage limitation. The whole strategy is implemented under the SM theory in contrast with other proposals that combine different strategies and do not provide all these operating modes. This characteristic offers the robustness of SM control and flexibility to easily get different operation modes. With this aim, different sliding surfaces are combined resulting in a single switching control law. Thus, the system is able to run from a zero energy stored state, exchange power with the microgrid in normal operation and shut down without the necessity of human intervention. The controller changes automatically between these modes, taking into account the references sent by the MGCC. A stability analysis and experimental results at maximum operating conditions are also presented. To the best of our knowledge, the control of a supercapacitor in the previously mentioned way, in the microgrid context and with exhaustive experimental tests, is not treated deeply in the bibliography.

The article is organized as follows. The next section describes the ESS based on a super-capacitor and presents the converter topology. In Section III, the proposed control strategy is introduced. Then, in Section IV, some aspects related to the implementation are discussed and in Section V experimental results are presented. The article ends with some concluding remarks.

II. Energy Storage Systems Based on Supercapacitors

Figure 1 presents a schematic view of the interface topology adopted to control the power flow between the Energy Storage Device (ESD) and the microgrid. It consists of an inverter connected to the grid (GSC), a DC link, a bidirectional DC/DC converter (ESSC) and the ESD. The last one is the physical device used to store energy (supercapacitors in the present work). Other types of ESD, such as Li-on batteries, can be used with the same topology and a similar control strategy.

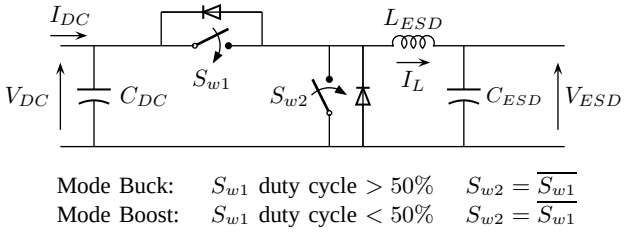

Fig. 2. Bidirectional DC-DC topology used in the ESSC

In grid connected microgrids, the objective of the controller of the GSC, K_{GSC}, is to ensure the power interchange between the ESD and the microgrid. To this end, the controller regulates the DC link voltage V_{DC} by injecting or by consuming power from the grid to maintain the power balance on the DC link.

The controller of the ESSC, K_{ESSC}, regulates the power exchanged between the ESD and the DC link. The controller designs strongly depend on the configuration of the microgrid at which the ESS is connected, as well as on the particular ESD used. In the configuration of Figure 1, K_{ESSC} receives instructions from the MGCC (in the form of a power reference, P_{ref}), which determines when the ESS must store energy and when it must inject energy into the grid. Figure 2 presents the bidirectional DC/DC topology adopted to implement the ESSC. For this topology, voltage is always higher on the left side (V_{DC}) than on the right side (V_{ESD}), but energy can flow in both directions. This converter can work in buck mode delivering energy to the storage device or in boost mode draining energy from the storage device. Each operating mode is achieved by setting the proper duty cycle on each switch. Switches S_{w1} and S_{w2} are operated in a complementary manner. This switching scheme avoids discontinuous operation for low current set-points. In both modes, the anti-parallel diodes act as free-wheeling diodes.

The DC link provides a certain degree of decoupling between both converters, permitting the design of each controller separately. Commonly, the GSC in grid connected mode is controlled with a cascaded control scheme. For details on the control of the GSC, see [10]–[12]. The controller of the ESSC is described in detail in the next section.

III. Sliding Mode Control of the ESS

Clearly, the system in Figure 2 is a variable structure system (VSS), *i.e.*, a system with dynamic changes in the conduction state of the switches. It is well known that sliding mode (SM) techniques provide quite effective control strategies in the case of VSS [13], [22].

For control algorithms, such as SM control, an instantaneous model of the switches is utilized. From Figure 2, it is possible to see that the structure and dynamics of the system strongly depend on the switch conducting state, even the energy flow direction can be changed with the switch operation. Actually, the DC/DC converter can be seen as formed by two subsystems (buck and boost) that can be selected according to the duty cycle applied to the switches S_{w1} and S_{w2}. These two operation modes can be synthetically described by the following unified model

$$\begin{cases} \dot{I}_L = -V_{ESD}/L_{ESD} + (V_{DC}/L_{ESD})S_w, \\ \dot{V}_{ESD} = I_L/C_{ESD}, \end{cases} \quad (1)$$

where C_{ESD} is the capacitance of the super-capacitor and

$$S_{w1} = S_w, \qquad S_{w2} = \overline{S_w},$$

where the overline denotes the logic inverse state, *i.e.* if $S_w = 1$ (switch closed) then $\overline{S_w} = 0$ (switch open). This equation represents the DC/DC converter dynamics for both operation modes. When the duty cycle of S_w is lower than 50%, the DC/DC converter works as buck and otherwise it works in boost mode.

The ESSC must fulfill several operation objectives depending on the microgrid and the supercapacitor states. Three clear objectives can be identified.

- Startup: the supercapacitors are charged from zero initial condition at constant current.
- Constant Power: I_L is controlled so that there is a power transfer from/to the grid according to a power reference P_{ref} imposed by the MGCC. Power mismatch between P_{ref} and the actual power transferred to the microgrid, due to power losses, is assumed to be compensated by the MGCC.
- Voltage Limitation: once V_{ESD} reaches the maximum or minimum operation voltage, V_{ESD} is maintained constant.

As mentioned above, these objectives are accomplished by the ESSC by controlling the inductor current I_L. In the rest of the section, it will be shown that these objectives can be achieved with a single, simple and easy to implement sliding surface whose reference is modified in correspondence with the pursued objective.

A. Startup

The target of this stage is to pre-charge the supercapacitors in order to be able to run automatically from a zero initial charge condition. To achieve this goal the current through inductor L_{ESD} is regulated at a constant value $I_{\max}$, the current limit of the supercapacitors. Here, the DC/DC converter works in buck mode. The following sliding surface

$$\mathcal{S}(I_L) = I_{\max} - I_L = 0 \quad (2)$$

is proposed associated with the switching logic

$$S_w = (\text{sign}(I_{\max} - I_L) + 1)/2, \quad (3)$$

where sign denotes the sign function. Then, it must be verified if (2) qualifies as a sliding surface, *i.e.*, if it satisfies the necessary and sufficient condition for sliding mode establishment, a.k.a. transversality condition ($\mathcal{L}_g\mathcal{S} = -V_{DC}/L_{ESD} < 0$), where $\mathcal{L}$ is the Lie derivative [13]. If this condition is fulfilled, it can be ensured that the state trajectories point toward the manifold from both sides. The existence condition can be obtained by the equivalent control method. The equivalent control is obtained from the invariance condition ($\mathcal{S} = 0$ and $\dot{\mathcal{S}} = 0$) and in the case of the switching law (3), the equivalent control is

$$S_{w_{eq}} = \frac{V_{ESD}}{V_{DC}}. \quad (4)$$

SM regimen exists on the manifold whenever the equivalent control satisfies that $0 \leq S_{w_{eq}} \leq 1$. That is, there exists SM on the manifold if $0 \leq V_{ESD} \leq V_{DC}$ (SM domain). This condition is always satisfied in the DC/DC converter topology in Figure 2.

The dynamics in SM is obtained by substituting S_w with the equivalent control in (1), resulting in

$$\begin{cases} \dot{I}_L = 0 \\ \dot{V}_{ESD} = I_{\max}/C_{ESD} \end{cases} \quad (5)$$

This equation reveals that there is no dynamics in the regulated current (positive constant current) and that the supercapacitor voltage increases linearly with time.

Notice that other current references can be used. Moreover, a similar SM control can be used to discharge the supercapacitor. In this case, the current reference is negative and the ESSC works in boost mode. Therefore, the switching logic is identical to (3) but now S_{w1}'s duty cycle is lower than S_{w2}'s. In this way, the system can be turned off for maintenance purposes, for example.

B. Constant Power

In this stage, the control law is similar to the previous case but the maximum current reference is substituted with the current needed to transfer the power demanded by the MGCC. The power reference depends on the particular microgrid operation and can be positive or negative. Therefore, the DC/DC converter must work in buck mode and boost mode to allow a bidirectional power transfer.

In this stage, the surface utilized is

$$\mathcal{S}(I_L) = \frac{P_{ref}}{V_{ESD}} - I_L = 0 \quad (6)$$

which verifies the transversality condition since $-V_{DC}/L_{ESD} < 0$ holds. Hence, the switching logic

$$S_w = (\text{sign}(\frac{P_{ref}}{V_{ESD}} - I_L) + 1)/2 \quad (7)$$

ensures the SM regimen.

The equivalent control results

$$S_{w_{eq}} = \frac{V_{ESD}}{V_{DC}} - \frac{P_{ref}^2 L_{ESD}}{V_{ESD}^3 C_{ESD} V_{DC}}. \quad (8)$$

The SM domain, $P_{ref}^2 L_{ESD}/V_{ESD}^3 C_{ESD} \leq V_{ESD} \leq V_{DC} + P_{ref}^2 L_{ESD}/V_{ESD}^3 C_{ESD}$, is always accomplished.

The dynamics during the SM regimen is obtained by substituting (8) in (1) and is given by

$$\begin{cases} \dot{I}_L = -\dfrac{I_L^3}{P_{ref} C_{ESD}}, \\ \dot{V}_{ESD} = \dfrac{I_L}{C_{ESD}} = \dfrac{P_{ref}}{V_{ESD} C_{ESD}}. \end{cases} \quad (9)$$

The trajectory of the states in SM regimes is illustrated in Figure 3. It can be observed that for all positive values of

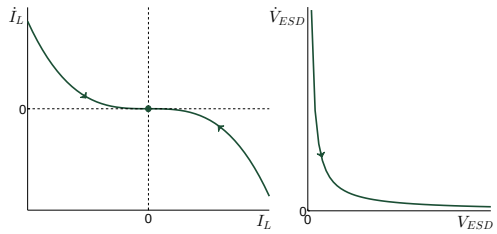

Fig. 3. SM dynamics in constant power

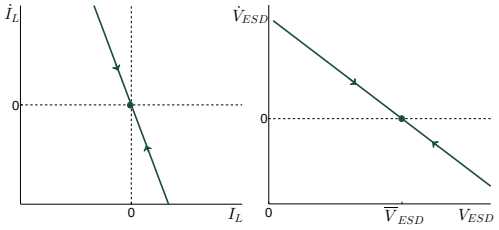

Fig. 4. SM dynamics in voltage limitation mode

I_L, its derivative is negative and for all for negative values, its derivative is positive. Therefore, from all initial conditions, the inductor current converges to the stable equilibrium point $I_L = 0$. For the supercapacitor voltage, its derivative is always positive (for positive inductor currents, buck mode) and then V_{ESD} will increase if the power reference remains with positive values. This is a characteristic of the system and is independent of the control strategy. For this reason, a voltage limitation mode is necessary to prevent the supercapacitor from being damaged, which is explained in the next subsection.

In both modes, the switching law is the same whether working as buck delivering energy to the storage device or working as boost consuming energy from the storage device. This is because of an inversion of the sign in the inductor current and reference.

Remark 1: It is important to note that the surface remains as a current surface. The only difference is that the reference is shaped dynamically.

C. Voltage Limitation

For operative and safety reasons, supercapacitors must operate within a voltage range limited by upper $\overline{V}_{ESD}$ and lower $\underline{V}_{ESD}$ limits. The upper limit is to protect the integrity of the supercapacitors. The lower limit is due to the fact that the supercapacitors cannot store much energy below this voltage and also, high current references could arise for high power references. To guarantee that these values are reached smoothly, an additional sliding surface is proposed, which is applied when V_{ESD} is in the transition regions $\mathcal{R}_l := \{V_{ESD} | \underline{V}_{ESD} < V_{ESD} < \underline{V}_{ESD} + V_\Delta\}$ and $\mathcal{R}_u := \{V_{ESD} | \overline{V}_{ESD} - V_\Delta < V_{ESD} < \overline{V}_{ESD}\}$, where V_Δ defines the width of the transition regions.

Therefore, when the supercapacitor voltage is in the transition region $\mathcal{R}_u$, the sliding surface is

$$\mathcal{S}(I_L) = \frac{P_{ref}(\overline{V}_{ESD} - V_{ESD})}{(\overline{V}_{ESD} - V_\Delta)V_\Delta} - I_L = 0, \qquad (10)$$

which verifies the transversality condition since $-V_{DC}/L_{ESD} < 0$ holds. In this case, the switching logic is given by

$$S_w = (\text{sign}\left(\frac{P_{ref}(\overline{V}_{ESD} - V_{ESD})}{(\overline{V}_{ESD} - V_\Delta)V_\Delta} - I_L\right) + 1)/2. \qquad (11)$$

The equivalent control results

$$S_{w_{eq}} = \frac{V_{ESD}}{V_{DC}} - \frac{P_{ref}^2 L_{ESD}(\overline{V}_{ESD} - V_{ESD})}{(\overline{V}_{ESD} - V_\Delta)^2 V_\Delta^2 C_{ESD} V_{DC}}. \qquad (12)$$

The SM domain is $\frac{P_{ref}^2(\overline{V}_{ESD}-V_{ESD})L_{ESD}}{(\overline{V}_{ESD}-V_\Delta)^2 V_\Delta^2 C_{ESD}} < V_{ESD} < \frac{V_{DC}+P_{ref}^2(\overline{V}_{ESD}-V_{ESD})L_{ESD}}{(\overline{V}_{ESD}-V_\Delta)^2 V_\Delta^2 C_{ESD}}$ that is always accomplished.

Substituting (12) in (1), the dynamics in the SM regimen can be obtained

$$\begin{cases} \dot{I}_L = -\dfrac{P_{ref}}{(\overline{V}_{ESD} - V_\Delta)V_\Delta}\dfrac{I_L}{C_{ESD}}, \\ \dot{V}_{ESD} = \dfrac{P_{ref}}{C_{ESD}(\overline{V}_{ESD} - V_\Delta)V_\Delta}(\overline{V}_{ESD} - V_{ESD}). \end{cases} \qquad (13)$$

These expressions can be seen in Figure 4. It is clear that for all initial conditions, the current approaches the stable equilibrium point $I_L = 0$. In addition the supercapacitor voltage converges to the final value $V_{ESD} = \overline{V}_{ESD}$ without overpassing the limit, whereas the inductor current goes to zero smoothly.

In the case of a negative power reference, the ESSC operates in boost mode. In this circumstance, when the voltage reaches the lower transition region $\mathcal{R}_l$, a switching law similar to (11) can be used.

Notice that this operating mode is necessary, first, to avoid dissconnecting the inductor when non-zero current is flowing through it, and second, to compensate supercapacitor losses, for example, if the system does not absorb energy for a long period of time.

D. Complete control strategy

Observing the SM surfaces (2), (6) and (11), it is clear that the different operation objectives can be fulfilled with the same switching law

$$S_w = (\text{sign}(I_{ref,i} - I_L) + 1)/2$$

with

- startup
$$I_{ref1} = I_{\max}, \qquad (14)$$
- constant power mode
$$I_{ref2} = P_{ref}/V_{ESD}, \qquad (15)$$
- voltage limitation mode (lower limit)
$$I_{ref3} = \frac{P_{ref}}{(\underline{V}_{ESD} + V_\Delta)V_\Delta}(V_{ESD} - \underline{V}_{ESD}), \qquad (16)$$
- voltage limitation mode (upper limit)
$$I_{ref4} = \frac{P_{ref}}{(\overline{V}_{ESD} - V_\Delta)V_\Delta}(\overline{V}_{ESD} - V_{ESD}). \qquad (17)$$

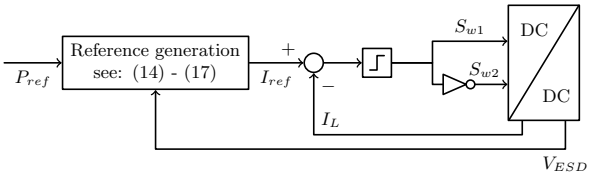

Fig. 5. Sketch of the proposed control strategy

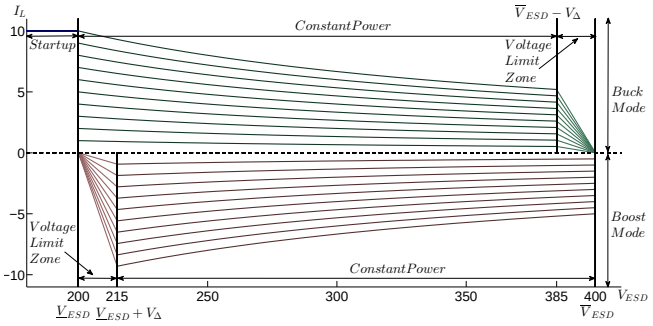

Fig. 6. Representation of sliding surfaces under the different operating modes and objectives

For the system startup, the control strategy imposes a constant current reference. The same surface, but with a negative reference can be utilized to discharge the supercapacitors. In constant power stage, the current reference is computed according to the current supercapacitor voltage in order to provide the amount of power indicated by the MGCC. Finally, when the supercapacitors reach the lower or upper voltage limits, a transition sliding surface is used to smoothly lead the inductor current to zero. A schematic representation of the control strategy is illustrated in Figure 5. In Figure 6, the different operating mode can be seen in the voltage-current plane.

Remark 2: In all cases there exists only one stable equilibrium point for the inductor current regulation. Therefore, from the previous analysis it can be concluded that the point is globally reached.

Remark 3: It is worth mentioning that the grid, the inverter along with the DC link capacitor and the controller K_{GSC} are considered a system that is perturbed by the rest of the system (ESSC). This consideration is a consequence of the robustness against variability of the DC link voltage and the supercapacitor voltage provided by the SM control. Hence, providing that a correct design of K_{GSC} ensures that the DC link voltage is higher than the maximum supercapacitor voltage plus the operation voltage of the converter (a requirement of DC-DC converter to work properly), the controller K_{ESSC} will work correctly (performance and stability) under SM control. This is one of the advantages of SM control.

IV. Experimental implementation

The proposed SM control strategy has been implemented in the set-up shown in Figure 7. The DC link voltage, V_{DC}, is set at 700 V, the inductance, L_{ESD}, is 4.27 mH and the DC link capacitance, C_{DC}, is 2 mF. The DC/DC converter has been implemented using IGBTs, with each IGBT rated at

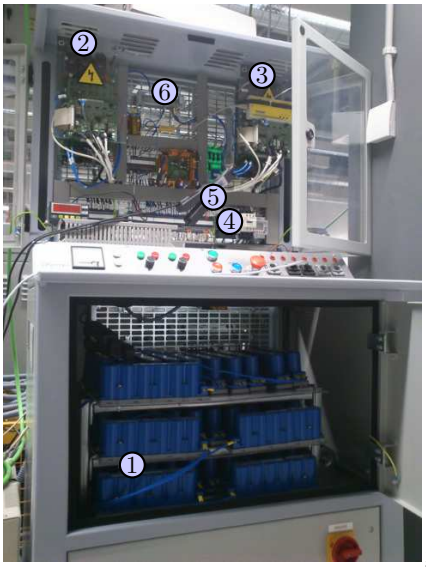

Fig. 7. Experimental set-up for the implementation of the proposed SM control strategy. (1) supercapacitor bank, (2) DC/DC converter, (3) grid side converter, (4) protections, (5) current prove, (6) DC link

TABLE I
Parameter values of the super-capacitor bank

Parameter name	Value
Absolute Max. voltage, $\overline{V}_{ESD_{MAX}}$	567 V
Max. operating voltage, $\overline{V}_{ESD}$	400 V
Min. operating voltage, $\underline{V}_{ESD}$	200 V
Max. output current, $I_{\max}$	19 A
Max. Peak Current, 1 s (non repetitive), $\overline{I}_{\max}$	200 A
Capacity, C_{ESD}	1.702 F

20 A maximum. The firmware has been written using ANSI-C language, compiled with speed optimizations, running on a TMS320F2808 DSP.

The GSC shown in Figure 1 is not the main contribution of this work. A detailed explanation of the control algorithm and the implementation can be found in [12], [23]. Notice that the switching frequency of the GSC is 12 kHz, higher than the maximum switching frequency produced by the SM controller. Different switching frequencies on both converters helps to reduce noise on the sampled signals. This noise is produced by the electromagnetic interferences between the converters. The supercapacitor bank is composed of thirty five MAXWELL BMOD0058 E016 B02 modules of 16.2 V and 58 F each, connected in series. For safety reasons, the bank has a maximum operating voltage of 400 V and a capacity of 1.7 F. Table I summarizes the main parameters of the supercapacitor bank.

A. Control algorithm

The control algorithm implemented in the DSP can be summarized in the following pseudocode.

while $(V_{ESD} < \underline{V}_{ESD})$ **do** ▷ Startup
  $S_w = (\mathrm{sign}(I_{ref1} - I_L) + 1)/2$

end while

Shutdown=FALSE

while (shutdown=FALSE) **do**

Read V_{ESD}

if ($V_{ESD} > \overline{V}_{ESD} - V_{\Delta}$) **AND** ($P_{ref} > 0$) **then**
▷ Voltage Limitation
$S_w = (\text{sign}\,(I_{ref4} - I_L) + 1)/2$
else if ($V_{ESD} < \underline{V}_{ESD} + V_{\Delta}$) **AND** ($P_{ref} < 0$) **then**
▷ Voltage Limitation
$S_w = (\text{sign}\,(I_{ref3} - I_L) + 1)/2$
else if ($\underline{V}_{ESD} < V_{ESD} < \overline{V}_{ESD}$) **then**
▷ Constant Power
$S_w = (\text{sign}\,(I_{ref2} - I_L) + 1)/2$
end if

if ($V_{ESD} > \overline{V}_{ESD} + V_{\Delta}$) **then** ▷ Protection
Shutdown=TRUE
end if

if ($V_{ESD} < \underline{V}_{ESD} - V_{\Delta}$) **then** ▷ Protection
Shutdown=TRUE
end if

end while

For the DC/DC converter in the implementation, the pre-charge current I_{ref1} is set to 10 A, the maximum operating voltage $\overline{V}_{ESD}$ to 400 V, the minimum operating voltage $\underline{V}_{ESD}$ to 200 V and the voltage threshold V_{Δ} to 15 V. Current references are computed using equations (14) to (17).

V. Experimental Results at Full Ratings

Three scenarios were analyzed in order to evaluate the proper operation of the proposed ESS: the startup, the tracking of several power references and the voltage limitation. For the experiment, the converter was operated at its nominal values to evaluate the proposed control strategy in a real situation.

Startup

During the startup scenario, the supercapacitors were pre-charged at constant current until a minimum operating voltage was reached. Figure 8 shows the current and the voltage in this scenario. The supercapacitor pre-charge current set-point was 10 A. It can be seen in Figure 8 that the controller achieves a suitable regulation of the current at the desired set-point. The minimum current ripple amplitude is a consequence of the hysteresis band used in the SM control, the inductance L_{ESD} and the voltage difference between V_{ESD} and V_{DC}. The ripple setting of the controller (ΔI) is 3.5 A, shown with dashed lines.

Figure 9 presents a detail of the current to show the reaching mode. This is the current trajectory starting from the initial conditions $I_L = 0$ to the SM surface $\mathcal{S}(I_L) = 10\text{ A} - I_L = 0$. The current slightly overpasses the hysteresis band as a result of the limited sampling frequency of the DSP and also measure noise. From Figure 9 it is possible to see that the current slope

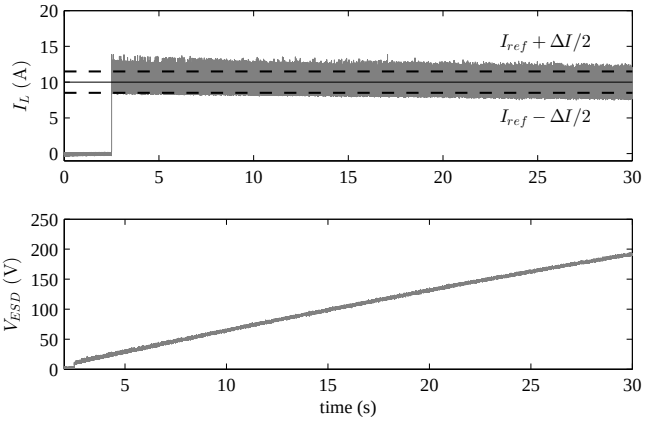

Fig. 8. Current I_L during pre-charge stage. Dashed lines are the bounds of the current ripple. The voltage of the supercapacitor bank is raised from 0 V to $\underline{V}_{ESD}$ (200 V).

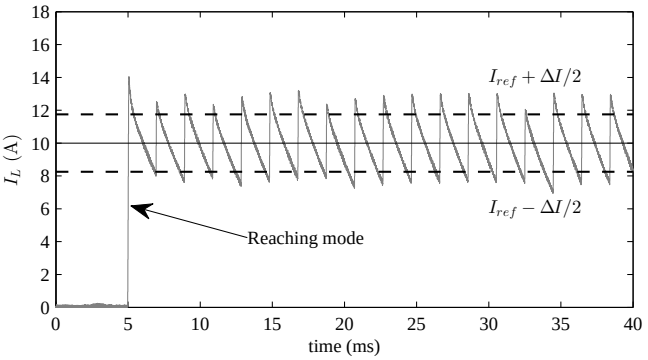

Fig. 9. Detail of the reaching mode during the system startup. Dashed lines are the bounds of the current ripple

when S_{w1} is closed is much larger than when open. If the current rises too fast, the DSP is not able to achieve an acute computation of the switching law (3). The slope of the current depends on the voltage difference between the supercapacitors and the DC link. Therefore, the phenomenon is more noticeable at the initial state, where the voltage difference between supercapacitors and the DC link is very high, in this case 700 V. This fast variation of the current results in a small delay in the detection of the crossing of the current with the upper limit of the hysteresis band. This is a limitation of the hardware employed, although the performance is suitable for the selected application. This phenomena is evidenced in Figure 8. When the supercapacitor voltage approaches the operating values, the current better fits the desired ripple bands. It is important to note that the startup stage is not a permanent mode of operation and the performance achieved is suitable for the discussed application.

Constant Power

The usual operation of the supercapacitors on the microgrid is to track the power set-points given by MGCC. The power is measured as the product of the supercapacitor voltage times the current flowing through the inductor L_{ESD}. By convention, positive power means that the power is being

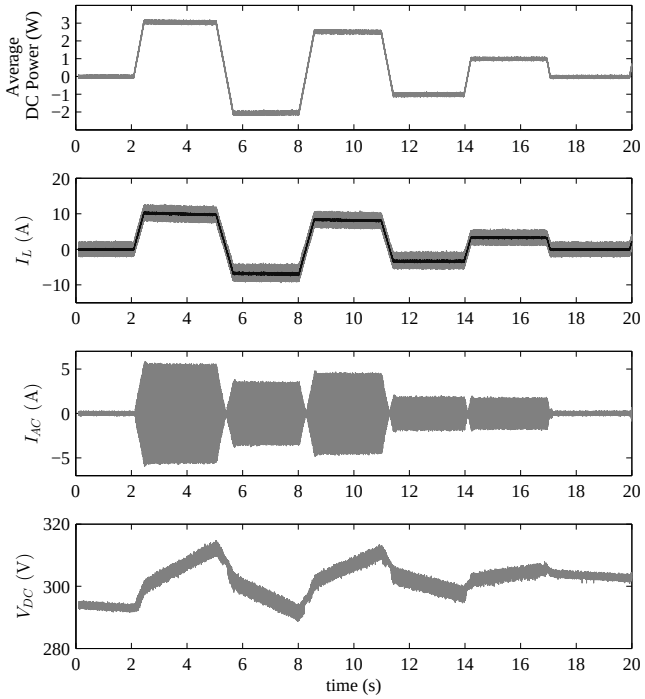

Fig. 10. Extract of most relevant states of the converter during normal operation. From top to bottom, the measured states are: average supercapacitor DC power, I_L current, AC current corresponding to phase-a of a tri-phase system and the voltage of supercapacitor bank

transferred from the DC link to the supercapacitors, and vice-versa, negative power means that the power is being supplied to the DC link. The average supercapacitor power is shown in Figure 10, as the interest of this application is on the mean value of the transferred power. Notice that the actual power transferred to the grid is lower than the supercapacitor power due to power losses.

The gray line of the I_L current in Figure 10 is the instantaneous current flowing through the DC inductor, and the black line is the current reference I_{ref}. It can be seen that I_L converges rapidly to the new SM surface when there is a change in the power reference. To show that the AC power consumed or injected to the microgrid is kept constant, Figure 10 shows the phase-a AC current during the tracking of six different power set-points, $P_{ref_1} = 0$ kW, $P_{ref_2} = 3$ kW, $P_{ref_3} = -2$ kW, $P_{ref_4} = 2.5$ kW, $P_{ref_5} = -1$ kW, $P_{ref_6} = 1$ kW. As a consequence of the current ripple, the super-capacitor bank voltage also has a small ripple.

It must be noted that although the SM controller is capable of an extremely fast transition between sliding surfaces with the reaching mode, the hardware of the experimental set-up cannot withstand such an abrupt change on the current flowing into the DC link, resulting in trips of the protections. For this reason the transition between different power set-points has been implemented with a ramp. The transition is fast and presents no overshoot. The tracking error is zero since the SM control strategy ensures zero steady state error.

A close lookup of the AC and DC currents of the converter are shown in Figure 11. The current I_L presents a constant

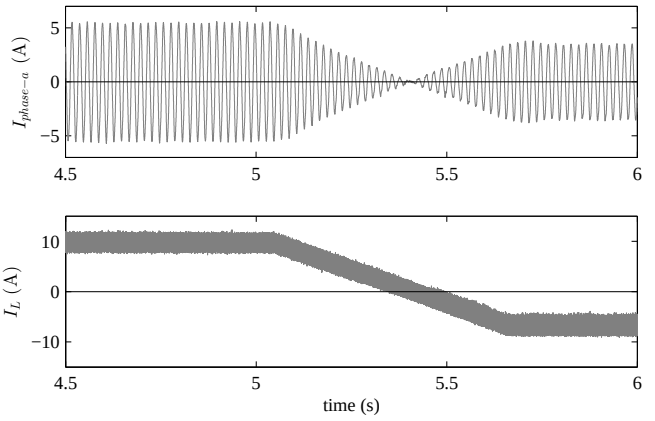

Fig. 11. Detail of the phase-a AC current and the DC I_L current during a sign change in the power flow.

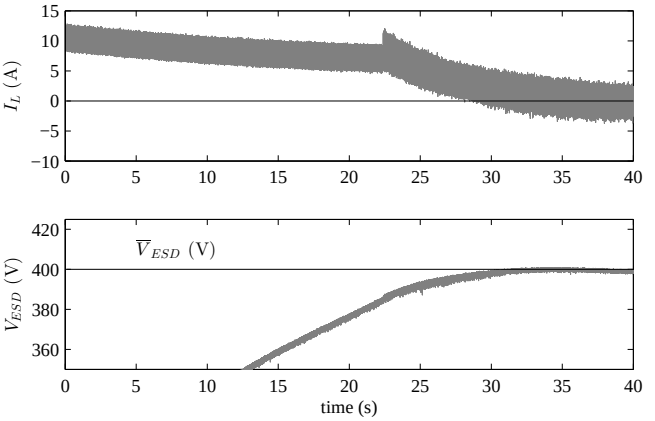

Fig. 12. Detail of the current I_L and voltage V_{ESD} during the voltage limitation mode.

ripple imposed by the hysteresis band of the sliding mode controller. The minimum current ripple and maximum switching frequency are a consequence of the DC inductance L_{ESD}, the voltage difference between the V_{ESD} and V_{DC}, and the sampling frequency of the controller. For this experimental set-up, the average current ripple is about 15% of the current limit and the switching frequency varies form 8 kHz to 11 kHz during normal operation. If lower ripple or higher frequency are required, some of the aforementioned parameters should be improved.

Voltage Limitation

The sliding surface defined in (10) is responsible for driving V_{ESD} to $\overline{V}_{ESD}$ smoothly and with no overshoot. The results of the implementation of the surface are shown in Figure 12. The supercapacitor voltage V_{ESD} is kept at 400 V ($\overline{V}_{ESD}$) in this experiment, guaranteeing the integrity of the supercapacitor bank. The voltage is kept constant at $\overline{V}_{ESD}$, maintaining the supercapacitors at the desired capacity until a negative power reference is received from the MGCC. Upon the reception of the discharge command, the controller re-enters in the constant power stage, starting a new cycle.

VI. Conclusion

A new control strategy for a bidirectional AC/DC converter to control the power exchange between a supercapacitor bank and a grid connected microgrid was presented. The proposed strategy is based on a unique SM surface which is able to cover all the operating conditions, even the startup of the supercapacitor bank. Different current references, depending on the particular objective, were used to produce a commanding law for the switching devices. The proposed control is simple to implement in the DSPs commonly used in power converters and also ensures proper operation in different conditions, even under changes in the system parameters. Also, as the whole strategy is based on sliding mode techniques, no slope compensation is needed for duty cycles above 50% as is required in fixed frequency current mode control. The proper operation and robustness were experimentally corroborated. Several scenarios covering all operating conditions, including the startup and extreme situations in which the supercapacitor reaches the maximum voltage, were analyzed. These results show that the proposed control strategy exhibits a suitable performance even in the presence of adverse conditions. Some hardware limitations can affect the system performance (ripple levels), especially during the startup. These limitations can be circumvented by increasing the inductor and using a more powerful ADC/DSP. This is a limitation of the laboratory hardware that can be avoided with non-expensive modifications in the equipment. Nevertheless, in microgrid applications such improvement in the ripple level might not be necessary.

VII. Acknowledgments

We thank Prof. Christopher Young for helping us with the presentation of our work.

References

[1] N. Hatziargyriou, H. Asano, R. Iravani, and C. Marnay, "Microgrids," *IEEE Power Energy Mag.*, vol. 5, no. 4, pp. 78 –94, 2007.

[2] M. Barnes, J. Kondoh, H. Asano, J. Oyarzabal, G. Ventakaramanan, R. Lasseter, N. Hatziargyriou, and T. Green, "Real-world microgrids - an overview," in *Proc.of the IEEE Int. Conf. on SoSE*, 2007, pp. 1–8.

[3] A. Mehrizi-Sani and R. Iravani, "Potential-function based control of a microgrid in islanded and grid-connected modes," *IEEE Trans. Power Syst.*, vol. 25, no. 4, pp. 1883 –1891, 2010.

[4] A. Colet-Subirachs, A. Ruiz-Alvarez, O. Gomis-Bellmunt, F. Alvarez-Cuevas-Figuerola, and A. Sudria-Andreu, "Centralized and distributed active and reactive power control of a utility connected microgrid using IEC61850," *IEEE Systems Journal*, vol. 6, no. 1, pp. 58 –67, 2012.

[5] A. Ruiz-Alvarez, A. Colet-Subirachs, F. Alvarez-Cuevas Figuerola, O. Gomis-Bellmunt, and A. Sudria-Andreu, "Operation of a utility connected microgrid using an IEC61850-based multi-level management system," *IEEE Trans. on Smart Grid*, vol. 3, no. 2, pp. 858 –865, 2012.

[6] N. Hatziargyriou, N. Jenkins, G. Strbac, J. A. Peças Lopes, A. Engler, J. Oyarzabal, G. Kariniotakis, and A. Amorim, "Microgrids - Large Scale Integration of Microgeneration to Low Voltage Grids," in *Proc. of the CIGRE C6-309*, 2006.

[7] F. Katiraei and M. Iravani, "Power Management Strategies for a Microgrid With Multiple Distributed Generation Units," *IEEE Trans. Power Syst.*, vol. 21, no. 4, pp. 1821–1831, 2006.

[8] A. Etxeberria, I. Vechiu, H. Camblong, and J.-M. Vinassa, "Comparison of three topologies and controls of a hybrid energy storage system for microgrids," *Energy Conversion and Management*, vol. 54, no. 1, pp. 113–121, 2012.

[9] F. Díaz-González, A. Sumper, O. Gomis-Bellmunt, and R. Villafáfila-Robles, "A review of energy storage technologies for wind power applications," *Renewable and Sustainable Energy Reviews*, vol. 16, no. 4, pp. 2154–2171, 2012.

[10] N. Pogaku, M. Prodanovic, and T. Green, "Modeling, analysis and testing of autonomous operation of an inverter-based microgrid," *IEEE Trans. on Power Electronics*, vol. 22, no. 2, pp. 613 –625, 2007.

[11] A. Yazdani and R. Iravani, *Voltage-sourced converters in power systems*. John Wiley & Sons Inc., 2010.

[12] F. D. Bianchi, A. Egea-Alvarez, A. Junyent-Ferr, and O. Gomis-Bellmunt, "Optimal control of voltage source converters under power system faults," *Control Eng. Practice*, vol. 20, pp. 539–546, 2012.

[13] V. Utkin, J. Guldner, and J. Shi, *Sliding Mode Control in Electro-Mechanical Systems, Second Edition*. CRC Press, 2009.

[14] H. Sira-Ramírez, "On the dynamical sliding mode control of nonlinear systems," *Int. Journal of Control*, vol. 57, no. 5, pp. 1039–1061, 1993.

[15] N. Vazquez, C. Hernandez, J. Alvarez, and J. Arau, "Sliding mode control for DC/DC converters: a new sliding surface," in *Proc. of IEEE ISIE*, vol. 1, 2003, pp. 422 – 426.

[16] F. Bianchi, H. De Battista, and R. Mantz, "On the stability of DC-to-DC converters in PV systems undergoing sliding motions," *Int. Journal of Systems Science*, pp. 637–647, 2004.

[17] A. El Aroudi, B. Robert, and R. Leyva, "Sliding mode control of a high voltage DC-DC buck converter," in *Proc. of the European Conference onCircuit Theory and Design*, vol. 3, 2005.

[18] A. M. Gee, F. V. P. Robinson, and R. W. Dunn, "Analysis of battery lifetime extension in a small-scale wind-energy system using supercapacitors," *IEEE Trans. Energy Convers.*, vol. PP, no. 99, pp. 1–10, 2013.

[19] S.-C. Tan, Y. Lai, and C. Tse, "An evaluation of the practicality of sliding mode controllers in DC-DC converters and their general design issues," in *Proc. of the 37th IEEE PESC*, 2006, pp. 1 –7.

[20] F. Ciccarelli and D. Lauria, "Sliding-mode control of bidirectional DC-DC converter for supercapacitor energy storage applications," in *Proc. of the Int. SPEEDAM*, 2010, pp. 1119 –1122.

[21] F. A. Inthamoussou, R. J. Mantz, and H. D. Battista, "Flexible power control of fuel cells using sliding mode techniques," *Journal of Power Sources*, vol. 205, no. 0, pp. 281 – 289, 2012.

[22] W. Perruquetti and J. P. e. Barbot, *Sliding Mode Control in engineering*. Marcel Dekker, 2002.

[23] L. Trilla, F. Bianchi, and O. Gomis-Bellmunt, "Optimal control of VSC for STATCOM applications," in *Proc. of PPPSC Symposium*, 2012.

Fernando A. Inthamoussou received the B.S.E.E. degree at the National University of La Plata (UNLP), Argentina, in 2009. He is currently pursuing his Ph.D at the Laboratory of Industrial Electronics, Control and Instrumentation (LEICI, UNLP, La Plata, Argentina). At present, he is a National Research Council (CONICET) Fellow and Assistant Professor at the EE Dept., UNLP. His main research interests are in nonlinear control of renewable energy systems, including robust, LPV and sliding mode control.

Jordi Pegueroles-Queralt was born in Barcelona, Catalunya in 1987. He received the M.Sc. degree in Engineering from the Technical University of Catalunya, Barcelona, Spain, in 2011, with the Master's Thesis given by the Politecnico di Torino, Italy. He was with the Humanoid-Lab group at the Institut de Robòtica i Informàtica Industrial from 2007 to 2011. Currently he is pursuing a Ph.D. degree at Catalonia Institute for Energy Research, Spain. His research interests are control theory applied to power electronics and renewable power sources.

Fernando D. Bianchi received the B.S. and Ph.D. degrees in electronic engineering from the National University of La Plata (UNLP), Argentina, in 1999 and in 2005, respectively. From 1999 to 2006, he was a Ph.D. student and a Postdoctoral Fellow at the Laboratory of Industrial Electronic, Control and Instrumentation (LEICI, UNLP, La Plata, Argentina). From 2006 to 2010, he was a Postdoctoral Researcher at the Technical University of Catalonia, Barcelona, Spain. In 2010, he joined the Power Electronics and Electric Power Grids Group, Catalonia Institute for Energy Research (IREC), Barcelona, as a Scientific Researcher. His main research interests include robust control and linear parameter-varying systems and their applications to the control of renewable energy conversion systems.